Article

Not peer-reviewed version

Geochemistry and Mineralogy of Precipitates from Passive Treatment of Acid Mine Drainage: Implications for Future Management Strategies

Joaquín Delgado *, Olivia Lozano Soria, Diana Ayala-Muñoz, Domingo Martín, Cinta Barba-Brioso

Posted Date: 27 September 2024

doi: 10.20944/preprints202409.2134.v1

Keywords: AMD treatment; Divalent metal carbonate; Jarosite-Alunite group; Waste management

Article

Geochemistry and Mineralogy of Precipitates from Passive Treatment of Acid Mine Drainage: Implications for Future Management Strategies

Joaquín Delgado [1,*], Olivia Lozano [1], Diana Ayala [2], Domingo Martín [1] and Cinta Barba-Brioso [1]

[1] Department of Crystallography, Mineralogy and Agricultural Chemistry, University of Seville, 41071 Seville, Spain; jdelgado15@us.es (J.D.); olozano2@us.es (O.L.); dmartin5@us.es (D.M.); cbarba@us.es (C.B-B.)
[2] Faculty of Engineering and Applied Sciences - University of Las Americas., UDLA Park 170124, Quito, Ecuador; diana.ayala.munoz@udla.edu.ec (D.A.)
* Correspondence: jdelgado15@us.es; Tel.: +34-600722205

Abstract: Traditional **m**ining activities in Zaruma-Portovelo (SE Ecuador) have led to high concentrations of pollutants in the Puyango River due to acid mine drainage (AMD) from abandoned waste. Dispersed Alkaline Substrate (DAS) passive treatment systems have shown efficacy in neutralizing acidity and retaining metals and sulfates in acidic waters, achieving near 100% retention for Fe, Al, and Cu, over 70% for trace elements, and 25% for SO_4^{2-}. However, significant solid residues are generated, requiring proper geochemical and mineralogical understanding for management. This study investigates the fractionation of elements in AMD precipitates. Results indicate that trivalent metals (Fe, Al) form low-crystallinity oxyhydroxysulfate minerals such as schwertmannite and jarosite, which retain elements like As, Cr, Cu, Pb, and Zn through adsorption-coprecipitation. Sulfate removal occurs via salts like coquimbite and gypsum. Divalent metals are primarily removed through carbonate and bicarbonate phases, with minerals such as azurite, malachite, rhodochrosite, and calcite. Despite the effectiveness of DAS, leachates from the precipitates exceed regulatory thresholds for aquatic life protection, classifying them as hazardous and posing environmental risks. However, these residues offer opportunities for the recovery of valuable metals.

Keywords: AMD treatment; Divalent metal carbonate; Jarosite-Alunite group; Waste management

1. Introduction

Acid mine drainage (AMD) is referred as a water course with both high acidity and concentrations of metal/loids and sulfates [1] generated by the oxidative dissolution of metal sulfides in abandoned mining areas and uncontrolled tailing dumps. It is a major cause of hydrographic basin contamination [2]. AMD poses a worldwide concern in mining, creating extreme environmental impacts to be responsibly managed [3,4]. In this sense, several passive remediation techniques, including dispersed alkaline substrates (DAS) [4–7], have been designed to reduce their environmental impact. Passive treatments are currently growing for the restoration of abandoned mine areas since it does not requires the continuous addition of reagents and needs occasional maintenance with little energy consumption [8,9], resulting in an economical option for AMD remediation. This technology, especially DAS, has been successfully applied in medium and high acidity waters with high metal loads, and it is widely developed despite problems of saturation or decrease in effectiveness of the system in the medium term [10–14].

While a significant amount of research has been dedicated to the occurrence and treatment of AMD, there has been limited investigation into the assessment and proper management of post-treatment residues of AMD. These treatments generate solid metal-rich residues or sludge (AMDp, acid mine drainage precipitates) that are also qualified as wastes [4,15]. These present high variability in chemical composition and physical properties depending on the AMD treated [16], making it

 doi:10.20944/preprints202409.2134.v

difficult to control and predict their stabilities and environmental behaviour. In fact, they could generate drainage themselves with negative environmental impacts whether their storage conditions are non-stabilized. That is the importance of a proper management of the solid waste generated during the neutralization of AMD polluted sources [17]. According to the literature, the recommendation to store the residues is very varied, but many authors agree the residues are unstable and should be stored in a dry environment [15]. According to regulations, any contact with acidic or alkaline water and DAS residues must be avoided.

Standardized leaching tests are commonly used to characterize the potential release of contaminants from treatment wastes, such as pH control leaching procedure (TCLP) or sequential extraction procedure (SEP), used increasingly by more researchers to understand the main processes in the mine waste environment: sulfide oxidation and retention of mobilized elements by secondary minerals via sorption and/or coprecipitation processes [18–20]. In this sense, effectiveness extractants and detailed studies of environmental conditions have been tested [i.e., 21-22]. Additionally, according to [17], metal links in Fe-rich DAM have still not been enough investigated in multi-step passive treatment methods, despite their importance in management strategies. These studies could allow the evaluation of the various residues as hazardous waste [15–23] as well as the establishment of the potential valorization of such metals from mining residues [12].

In this context, the aims of the present study were: (1) to gain a better understanding of trace metal cycles in environmental systems affected by AMD., This objective was based on a detailed geochemical characterization of trace elements mobilized from the generated solid wastes (AMDp) in a laboratory passive multi-step treatment for Fe-rich AMD. (2) to investigate mineral transformation and its influence on element fixation, as a basis of future studies on waste reutilization and better management strategies for appropriate storage.

2. Study Area

Mining operations in southern Ecuador have had an impact on the Puyango River basin, a crucial basin that runs through southern Ecuador and northern Peru before reaching the Pacific Ocean [24]. During its initial stretch, Puyango River flows through the Zaruma-Portovelo gold mining site (ZPMS).

Climatic, geological and metallurgical characteristics, as well as environmental implications of mining operations at the Puyango watershed have been previously described by several authors [2, 26-29].

The polluted state of the lower Puyango basin was claimed by Peru government in 2008, in consideration of the Binational Convention Puyango-Tumbes (1971). Since then, Ecuadorian authorities have invested great efforts to improve the situation of the watershed [2].

3. Materials and Methods

3.1. Experimental Design and Sampling

A reactive substrate system (Figure 1) combining calcium and magnesium DAS according to the conceptual model developed by [14; 30], was implemented at the National Research Institute of Geology, Mining, and Metallurgy (INIGEMM) laboratories in Quito, Ecuador. AMD sources located at the ZPMS selected for treatment exhibited mean pH values of 2.7 and an electrical conductivity of 4.7 mS/cm, both indicative of high acidity (4361 mg/L eq as CaCO3 equivalents) and elevated concentrations of Al, Cd, Cu, Fe, Mn, Pb, Zn, and sulfates. The system operated at both low and high hydraulic flow rates during 8 months, proving high efficiency in increasing water pH and achieving approximately 80% retention of Fe, Al, Mn, and trace elements. A complete description of the design, results and the hydrochemical model can be found in [2; 26].

The dissolution of limestone sand promotes the reduction of protons in solution, which increases pH and induces the formation of an "ochre" horizon in the first few centimeters of the column due to chemical shock, followed by a white horizon that may correspond to Fe and Al precipitates, respectively [2]. DAS-Ca alone is probed to be insufficient to remediate high concentrations of

 doi:10.20944/preprints202409.2134.v

divalent metals such as Zn, Mn, Ni, and Cd derived from hydrochemical conditions [31–33]. For this reason, [34] conducted laboratory experiments demonstrating that caustic magnesia (MgO) could be used to remove high concentrations of divalent metals from solution.

To evaluate the effectiveness of the acid water treatment, solid waste (AMDp) generated in the columns at various depths was sampled after the treatment. Five samples were taken from the DAS-Ca column located at depths of 3.5, 7.5, 8.5, 10, and 15 cm, while four samples were collected from the DAS-Mg column: two samples coinciding with superficial green-white precipitates and two samples at 1 and 12 cm, respectively (Figure 1).

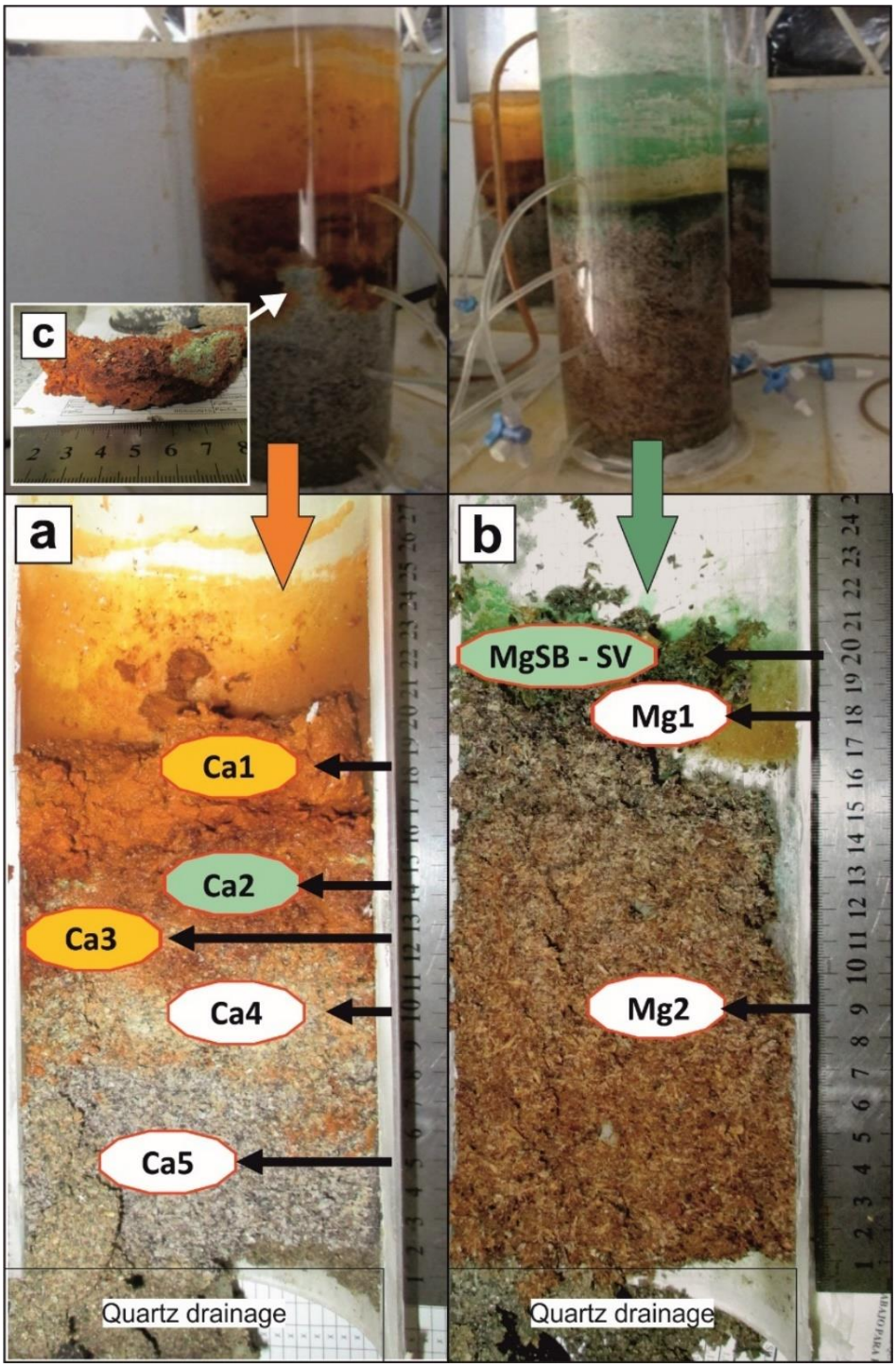

Figure 1. The passive treatment system based on the DAS concept [2]. Photographs of the sampling points in the DAS-Ca column (a), DAS-Mg column (b) taken after 8 months of treatment. (c) Detail of inner Ca2 layer showing green precipitates.

 doi:10.20944/preprints202409.2134.v

3.2. Chemical Study

Total element concentrations were determined as the sum of 5 steps of the selected SEP [35]. Sequential extractions are widely used for exploration purposes and to study element speciation in natural environments (i.e., [36,37]) and gradually more in mine wastes environment, to understand trace metal mobility. In this study, changes were implemented to the ratio of sample to extractant volume and to experimental settings for high concentrations of iron oxides and oxyhydroxysulfates [38,39]. Due to the presumable nature of samples, this study was performed according to [35] and the schematic SE steps are summarized in Table 1.

Major and trace elements were determined in < 0.2 μm extracted solutions by inductively coupled plasma-atomic emission spectroscopy (ICP-OES, model Optima 8300, Perkin Elmer). The main key elements (Ag, Al, K, Mg, Mn, As, Be, Ca, Cd, Co, Cr, Cu, Mo, Na, Nb, Ni, Pb, Sn, Sr and Zn) were reported. Calibration and accuracy controls were certified with ICP Multi-Element standard solutions from AccuStandard, SQS-01-1CRM, and SQS-02-R1-1CRM, according to the EPA 200.7 and EPA 6010. Certified reference material (No. 1244) and inter-laboratory tests for Trace Metals (No. 586) (CRM-European Environmental Production) were measured as quality controls. Each step of SEP was analyzed in triplicate, calculating the relative percentual difference (Eq. 1) among the replicates and the mean values. Most values were below the admissible value (5%), except for Ag, which stood at 10%.

$$\%RPD=(S-D)/(((S+D)/2)) \times 100 \quad \text{Eq.1}$$

Where: S = determined value of the samples, D = value of the duplicates.

The internal recovery of this SEP was assessed by comparing the sum of each metal in the five fractions with its acid-digested concentration, in percentage. Recovery rates for Al, Zn, Cu, Fe, and Mn ranged from 102.2% to 97.3%, 91.6% to 105.8%, 90.8% to 109.0%, 90.0% to 109.0%, and 91.4% to 107.4%, respectively.

Table 1. Five steps sequential extraction procedure scheme. *Correspond with the mineral phases dissolved in each step proposed by [35].

Sequential extraction step	* Dissolved phases	Elements released to the solution	Possible Dissolved phases
1. Water soluble fraction: 200 mg of sample and 20 ml deionized water, shake for 12 h at room temperature.	Gypsum	Ca and SO_4^{2-}; Also Fe, K, Mg, Mn, Zn, and Cd-Co	Gypsum, Secondary sulfates and other salts, hydroxides, Fe-amorphous
2. Sorbed and exchangeable fraction: 20 ml of 1 M NH_4-acetate (4.5 pH buffer), shake for 1 h at RT.	Calcite	Ca and adsorbed elements; Fe and Al-K, As, Cu, Mn, Zn	Metal-**divalent carbonate** type, including calcite; Fe-**amorphous** or very poorly ordered **Fe(III) precipitates**
3. Poorly ordered Fe(III) oxyhydroxides and oxyhydroxysulfates: 20 ml of 0.2 M NH_4-oxalate (3 pH buffer), 30 minutes shake in darkness at RT.	Schwertmannite, hydrobasaluminite, and gibbsite	Fe, Al, and SO_4^{2-} and trace associated Residual Ca	**Schwertmannite; jarosite-**Alunite group
4. *Highly ordered Fe(III) hydroxides and oxides*: 20 ml of 0.2 M NH_4-oxalate (3 pH buffer), 80°C water bath for 1 h.	Goethite	K, Fe, Al, and SO_4^{2-}; also As, Cu, Zn, Mn, Mg, Residual Ca	**Jarosite**-Alunite group; residual Ca-Mg-Mn oxides

 doi:10.20944/preprints202409.2134.v

5. Residue digestion: 3 ml of HNO_3 + 7.5 ml of HF + 2.5 ml of $HClO_4$	Residue (wood chips)	Organic elements	Wood and residual silicates and clay assimilated

3.3. Mineralogical Characterization

X-ray diffraction (XRD) measurements were performed with a Panalytical Empyrean diffractometer with Cu-Kα radiation at 40 kV and 20 mA. A step size of 0.008º 2θ was used in the range of 5-80°, and a step time of 0.5s/step was set. The software used for mineral identification were EVA v16.0 (Bruker-AXS) and Match! v3.15 (Crystal Impact), and the BGMN/Profex v4.8 for Rietveld refinement. bundle was employed. Structure models for Rietveld analysis were selected based on Powder Diffraction File database matches; the structures models used are sourced from the Crystallography Open Database. The crystallinity order of the analyzed samples was calculated using the software Diffract.Eva v4.1 (Bruker-AXS). This crystallinity order represents the proportion of crystalline material in the samples, as indicated by the total integrated areas of the full pattern. In samples with higher crystallinity, the refinement fit control values (such as discrepancy values, χ2, and agreement factors R, Rwp, Rexp and RB) were satisfactory. However, in samples with lower crystallinity and poor-quality data, these values were higher. This was why, due to the low crystallinity of some of the mineral phases present, the percentages of the mineral phases were semi-quantitative.

Selected samples were studied using a Tescan-MIRA 3 scanning electron microscope (SEM) operating with an accelerating voltage of 25 kV. Compositional information was extracted by back-scattered electron (BSE) imaging and energy dispersive X-ray (EDX) microanalysis (Link ISIS system). The samples were coated with a sputtering Quorum-Q150R ES with gold-platinum.

4. Results and Discussion

4.1. Metal Partition from AMD to Solid Phases

During the AMD treatment, the progressive increase of pH along the DAS-Ca column promoted the formation of an “ochre horizon” in the first centimeters of the solid residue followed by a “white horizon” (Figure 1a). Samples Ca1, Ca2, and Ca3 were taken from the first centimeters of the profile (3.5, 7.5, 8.5 cm, respectively), while samples Ca4 and Ca5 were collected in the white horizon (10 and 15 cm, respectively). The chemical conditions developed along the column, triggered Fe depletion from solution (Delgado et al., 2019), probably forming low-crystalline oxyhydroxides or oxy-hydroxysulfates. such as H-jarosite [(H3O)Fe3(SO4)2(OH)6], K-jarosite [KFe3(SO4)2(OH)6], schwertmannite [Fe8O8(OH)6(SO4)], ferrihydrite [Fe(OH)3], hematite [α-Fe2O3], goethite [α-FeOOH], lepidocrocite [γ-FeOOH], and maghemite [γ-Fe2O3].

Indeed, the "ochre horizon" (Figure 2a) exhibited the highest concentrations of Fe, with retention rates exceeding 90% (Ca1; 336 g/kg) and 80% (Ca3; 149 g/kg) of the total metal content (Figure 2a; Table 2), as confirmed by the corresponding visual observations. Lower Fe concentrations were measured in sample Ca2 (30 g/kg), accounting for 10% of the total element proportion. This can be attributed to significant dissolution of the calcium substrate and unexpected local alkaline conditions in this section of the DAS-Ca (Figure 1c). This is further supported by the high concentrations of Cu (42 g/kg) observed in this horizon profile, indicated by the presence of green precipitates (Figure 1c). These AMDp are commonly associated with the precipitation of divalent metal hydroxides, as described by [32], when the pH reaches neutral to alkaline conditions. This supports the high concentrations of Al (43 g/kg), Mg (1300 mg/kg), Mn (1223 mg/kg), and Zn (3860 mg/kg) in this layer of the profile.

The deeper 'white horizon' likely corresponds to Al precipitates formed when pH increases, as described by [14]. This is confirmed by the higher Al concentration through the column, with the highest value (56 g/kg) present in sample Ca4 (Table 2).

SEP data of the surficial sample, Ca1, indicates the presence of high concentrations of Ca (760 mg/kg). Besides, Ca increases at greater depths, so Ca3 shows 17 g/kg associated with the labile

 doi:10.20944/preprints202409.2134.v

fraction of the residues (Figure 2b,d, respectively). Furthermore, in the exchangeable fraction (F2), the release of low crystalline iron hydroxide seems evident, along with weakly adsorbed trace elements onto these compounds, as previously described other authors [40]. The presence of iron and trace metals in the F2 of sample Ca1 (Figure 2b) endorse this interpretation.

Table 2. Summary of the solid wastes pseudototal concentration showing the elements frequently associated with AMD environments in the Zaruma-Portovelo mine district. <d.l. Below detection limit.

Element	Das - Ca					Das - Mg	
(mg/kg)	Ca 1	Ca 2	Ca 3	Ca 4	Ca 5	Mg 1	Mg 2
Ag	9.74	23.23	16.33	36.15	100.76	11.82	60.00
Fe	336422	30527	149324	3096	2324	32842	727
Al	2497	43040	7091	56474	8288	1576	162
As	6616	127	1215	37.6	11.2	43.0	31.1
Ca	1085	145278	19878	160770	257355	11060	116385
Cd	39.6	0.71	9.75	<d.l.	34.7	5347	4453
Co	3.49	<d.l.	2.41	<d.l.	<d.l.	773	4565
Cr	118	21.4	28.6	14.0	19.2	20.2	68.4
Cu	423	41688	1015	4632	9842	909599	11385
K	2626	1227	1114	1672	3603	4023	943
Mg	290	1305	347	1330	2597	916	8253
Mn	107	1223	74	1024	2471	13181	75841
Mo	<d.l.	17.7	1.27	25.3	24.9	0.86	4.87
Na	745	554	492	579	1174	1257	460
Ni	4.01	12.4	2.29	1.49	<d.l.	486	1883
Pb	39.0	1.80	47.3	<d.l.	<d.l.	92.3	112
Sb	112	62.3	70.2	68.1	68.6	92.3	112
Sr	21.1	574	36	588	1130	69.8	1364
Zn	139	3860	86	320	517	517344	465916

The movement of trace elements from solution to solid Fe-Al phases involves adsorption and/or coprecipitation mechanisms. Research on ochre-like deposits rich in iron in acidic conditions indicates that jarosite and schwertmannite may have the greatest amounts of As and Cr [41], as well as other metals like Cu, Pb, and Zn [42]. Furthermore, ferrihydrite appears to be related to high concentrations of Pb and relatively high content of Zn and Ni [43]. In this regard, the main concentration of As associated with the higher concentration of Fe and K in samples Ca1 and Ca3 (Figure 2b,d) was determined, presumably associated to schwertmannite and jarosite. Contrary to expectations, although significant concentrations of As, Cu, and Pb associated with fractions F3 and F4 (involving Fe(III) oxyhydroxides and oxyhydroxysulfates) were leached, concentrations of up to 2536 mg/kg of As (e.g. Ca1 sample) were extracted in F2, the fraction associated with carbonates (Figure 2b). This could be attributed to the dissolution of amorphous or not ordered Fe(III) precipitates, along with the release of adsorbed elements such as As, Cu, Mn, and Zn, induced by the exposure to acetic acid at pH 4.5 within fraction F2. Additionally, excluding the samples from the DAS-Mg, trace metals Cu, Cd, Pb and Zn showed considerable concentrations associated with this section of the iron profile (up to 105, 38.1, 27.7 and 42.2 mg/kg, respectively), confirming the link between Fe-rich mineral phases and trace elements retention.

According to [15], aluminum may be trapped as hydroxides or hydroxysulfates in the white precipitates, which were mainly concentrated in sample Ca4, as shown in Figure 1a. The high Al concentrations extracted in F3 and F4 confirmed the dissolution of Al-rich sulphate phases such as alunite [KAl3(SO4)2(OH)6], basaluminite [Al4(SO4)(OH)10·5(H2O)], jurbanite [Al(SO4)(OH)·5(H2O)] or Al-hydroxides [Al(OH)3(am), gibbsite AlOH3, boehmite γ-AlO(OH), and diaspore AlO(OH)] that would be important as the pH rises above 6 [44-45; 25]. Furthermore, the

 doi:10.20944/preprints202409.2134.v

presence of alunite could be elucidated by considering the relative concentration of potassium in this profile section. Also, elevated concentrations of Cu, Ca, and Al detected in sample Ca2 seem to support this statement. These precipitates frequently contain gypsum (confirmed by the high concentration of Ca associated to F1 fraction, Figure 2c,e). Furthermore, according to the hydrochemical model developed by [2] in these sections of the profile, the dominant aqueous species (AlSO4+, Al(OH)2+ and AlOH+2) and the pH range between 5.8 and 6.4 are consistent with the precipitation of Al-phases.

It is noted that the neutral conditions obtained in the final section of the DAS-Ca are not usually enough for the formation of divalent metal hydroxides [32]. According to [46], the most effective retention of divalent metals is achieved when the pH is between 8 and 10 because important desorption processes can occur at higher pH values. Based on these premises, the presence of high concentration of Ca at the final section of the DAS-Ca (F2 of samples Ca4 and Ca5, Figure 2) added to the addition of alkalinity by the magnesia dissolved in the DAS-Mg (supported by the presence of Mg in the F1 of Ca5) appear to provide an ideal scenario for divalent metal retention. However, the control over the fractionation of divalent metals appears to be mainly exerted by carbonate phases [2]. These conditions were obtained towards the end of DAS-Ca (sample Ca5), were accompanied by significant concentrations of Ca, Mg, Cu, or Fe (until 231, 2.3, 9.4, and 1.7 g/kg, respectively) associated with the exchangeable phase (Figure 2f). Additionally, the fractionation of divalent elements in this zone of the profile seems to be somehow influenced by the availability of aluminum, with these phases extracted in F3 of the SEP, as previously suggested by [35].

The samples at 1 and 12cm in the DAS-Mg (Mg1 and Mg2, respectively) exhibited the highest concentrations of Cd, Co, Cu, Ni, Pb and Zn (Table 2 and Figure 2g-h). The DAS-Mg hydrochemical model indicated that the primary carbonate species in water quickly vanish upon entering the DAS-Mg column because of the formation of carbonate minerals [2], such as malachite [Cu3(CO3)2(OH)2], azurite and to a lesser extent smithsonite [ZnCO3:1H2O]. These premises are congruent with the results of the partitioning process observed in the experimental columns, where the main retention of Cu and Zn (900 and 516 g/kg, respectively) were associated with the sample Mg1 (exchangeable fraction, Figure 2g), which was supported by a noticeable change in color (bluish green) of the precipitates at the DAS-Mg surface. It is also important to note that most partition of Zn from solution to the solid phase occurred in the final section of the DAS-Mg, with Mg1 (around 40%) and Mg2 (80%) being the most significant (Figure 2a). In calcareous settings, when there are relatively high levels of divalent metals present (such as in the DAS- Mg column), the amount of these metals in water (including Cd and Mn) is typically controlled by the formation of solid metal-carbonate compounds through precipitation [47–49]. In fact, Zn and Mn showed a clear association with the carbonate fraction of the AMDp. Also, while Cd exhibits some association with water-soluble fraction along with Co (894 and 1360 mg/kg, respectively), its higher concentrations (3558 and 3202 mg/kg) appear to be associated with the F2 fraction (Figure 2h). Other divalent metal as Ni and Cr seems plot similar behavior associated with these fractions, showing their higher concentrations (e.g. Ni, 1878 mg/kg in F2, Figure 2h).

 doi:10.20944/preprints202409.2134.v

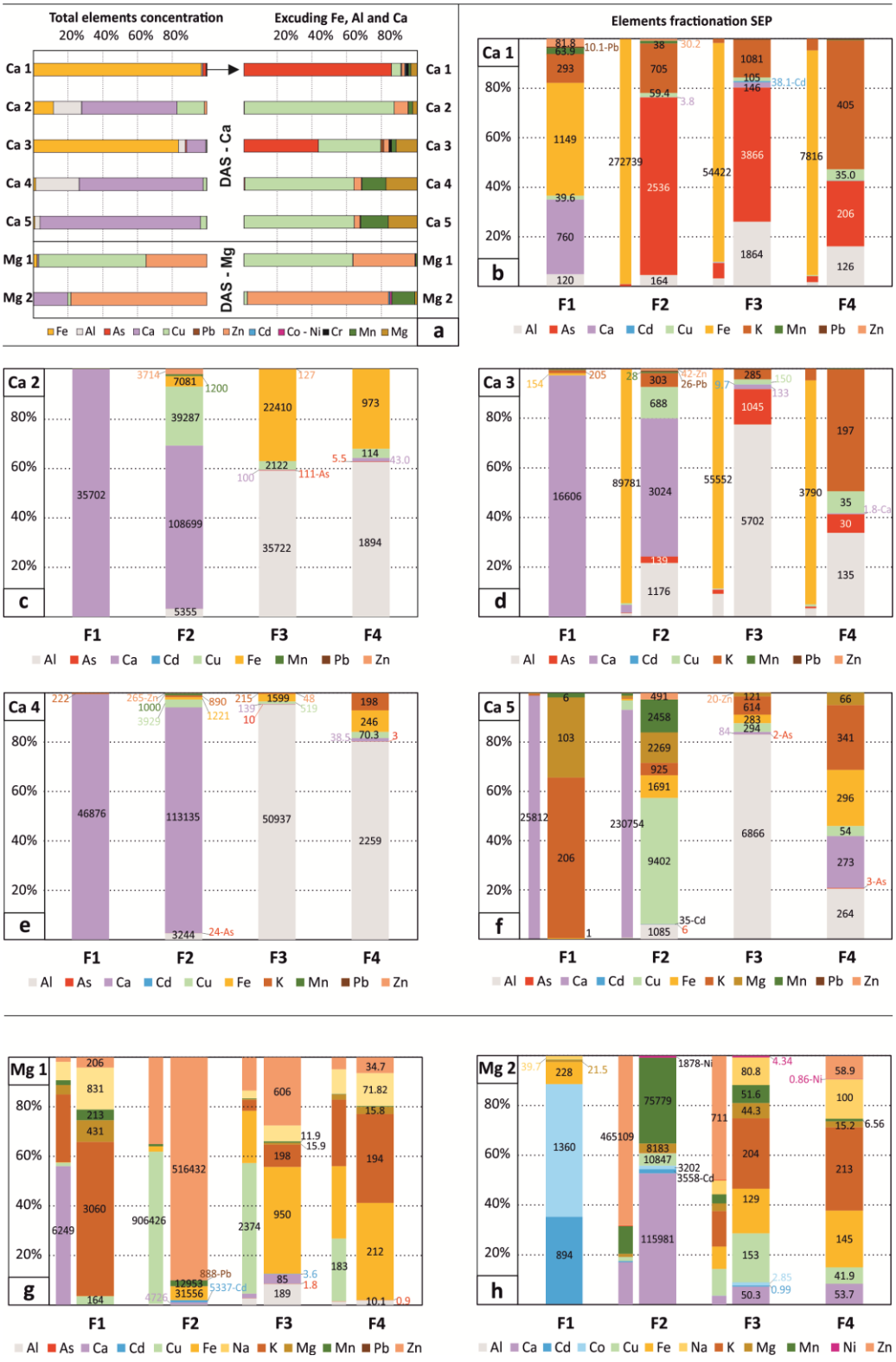

Figure 2. (a) Total concentration in each sample (% respect to total) of the main elements involved in the AMD neutralization process. (b-f) Sequential extraction data showing the percentage of the total extracted in each fraction. Where necessary, elements with higher concentrations have been suppressed (thin bars) to improve the visualization of trace elements. Concentrations are expressed in mg/kg.

 doi:10.20944/preprints202409.2134.v

4.2. DAS Mineralogical Assemblages

In the diffraction pattern of the surficial sample of DAS-Ca (Ca1), the presence of amorphous and low crystalline phases required background subtraction, so the peaks of some minerals become evident (Figure 3a).

Figure 3. Representative DRX pattern of samples in the DAS-Ca (Ca1) (a) and DAS-Mg (Mg1) (b), showing the main mineral phases identified and their correlation with the patterns obtained from database by Match.

In the "iron profile", the precipitation of the first oxyhydroxysulfates, such as schwertmannite and jarosite, could trap toxic elements like As, Cr, Cu, Pb, and Zn from solution [41,42]. According to [50], these are the controlling phases at low pH values. Observations by SEM-EDS showed a clear association between S and Al-Fe, and dissemination of As and Pb trapped in this column section (Figure 4a). Other sulphate species could play an important role here, depending on the availability of certain elements in the solution. The high proportion of Fe3+ in solution could led to coquimbite

 doi:10.20944/preprints202409.2134.v

formation (Fe3+2(SO4)3·9H2O), and if the water contains more than 1500 mg/L sulfate, the presence of gypsum is expected due to the dissolution of the reactive calcium across the substrate. Additionally, brushite (CaHPO4·2H2O) seems to crystallize under these conditions [51] in an AMD wetland restoration treatment. In this line, the hydrochemical data reported by [2; 26] suggest that during the initial acidity neutralization process at low pH, several phosphates could crystallize, including brushite (Figure 3a) and other not detected like monazite (La, Ce) which could retain REE from the solution.

Sample Ca2 (Figure S1, Supplementary Data), was dominated by amorphous phases, but also presented calcite and gypsum, which accounted 54% and 45% of the crystalline phases, respectively (Table 3). This sample corresponded to a zone of the profile where the nature of the alkaline reagent could be observed. However, the relatively high concentration of Cu, Zn (Figure 2c), and gypsum (rhombohedral) in this section seems to be a consequence of the beginning neutralization processes, as evidenced by the green-white color of the precipitates. In fact, the SEM images confirmed the presence of some Al-hydroxide amorphous precipitates and discrete Cu carbonated phases. Low presence of Fe associated to S and Al could explain the commonly described substitution Fe to Al in the Jarosite-Alunite group [52,53] as the pH increases (Figure 4b-c).

Table 3. Semiquantitative results made by Rietveld showing grade of crystallinity of the samples and chi^-2GOF obtained before analysis. DRX pattern and identification peek can be seem in the supplementary Figures (S1-S6). * Trace percentage (< 1%). Mineral symbol according to IMA–CNMNC [55].

		DAS-Ca					DAS-Mg		Drain
Mineral phases	**SAMPLE**	**Ca1**	**Ca2**	**Ca3**	**Ca4**	**Ca5**	**Mg1**	**Mg2**	**Pindo**
Boehmite	γ-AlO(OH) Bhm	-	-	3.4	-	-	-	-	-
Brushite	$Ca(PO_3OH) \cdot 2H_2O$ Bsh	9.5	-	5.9	-	-	-	-	-
Calcite	$CaCO_3$ Cal		54.5		51.6	85.6	-	59.2	-
Coquimbite	$AlFe_3(SO_4)_6(H_2O)_{12} \cdot 6H_2O$ Coq	22.1	-		-	-	-	-	-
Diaspore	AlO(OH) Dsp		-		1.2	-	-	-	-
Dolomite	Ca, Mg(CO3)2 Dol		-		3.0	-	42.9	-	-
Gypsum	CaSO4 Gp	2.4	45.5	74.1	44.2	13.7	2.0	-	-
Jarosite	$KFe^{3+}_3(SO_4)_2(OH)_6$ Jrs	14.7	-	6.9	-	-	-	-	-
Melanterite	$Fe^{2+}(H_2O)_6SO_4 \cdot H_2O$ Mln		-	4.0	-	-	-	-	-
Quartz	SiO_2 Qtz	15.9	-		-	0.7	1.9	0.6	72.0
Schwertmannite	$Fe^{3+}_{16}(OH,SO_4)_{12\text{-}13}O_{16} \cdot 10\text{-}12H_2O$ Swm	35.4	-	5.8	-	-	-	-	-
Aragonite	$CaCO_3$ Arg	-	-	-	-	-	-	34.1	-
Aurichalcite	$(Zn,Cu)_5(CO_3)_2(OH)_6$ Ach	-	-	-	-	-	11.6	-	-
Brucite	$Mg(OH)_2$ Brc	-	-	-	-	-	-	1.1	-
Malachite	$Cu_2(CO_3)(OH)_2$ Mlc	-	-	-	-	-	24.2	-	-
Monohydrocalcite	$CaCO_3 \cdot H_2O$ Mhcal	-	-	-	-	-	1.9	-	-
Rhodochrosite	$MnCO_3$ Rds	-	-	-	-	-	9.1	2.0	-
Siderite	$FeCO_3$ Sd	-	-	-	-	-	6.5	3.1	-
Albite	$Na(AlSi_3O_8)$ Ab	-	-	-	-	-	-	-	8.7
Chlorite	(Mg,Fe)3(Si,Al)4O10(OH)2(Mg,Fe)3(OH)6 Chl	-	-	-	-	-	-	-	4.0
Magnetite	$Fe^{2+}Fe^{3+}_2O_4$ Mag	-	-	-	-	-	-	-	1.0
Microcline	$K(AlSi_3O_8)$ Mcc	-	-	-	-	-	-	-	1.5
Mica	$K(Mg,Fe)_3AlSi_3O_{10}(OH,F)_2$ Mca	-	-	-	-	-	-	-	11.9
Orthoclase	$K(AlSi_3O_8)$ Or	-	-	-	-	-	-	-	1.0
Total		100.02	100.00	100.00	100.00	100.01	100.00	100.00	100.01
% Crystallinity		7.43	88.1	11.6	89.1	90.5	56.3	78.7	89.2
chi^2		18.8	2.12	13.6	3.27	4.11	1.56	3.97	1.41
GOF		4.34	1.45	3.69	1.81	2.03	1.25	1.99	1.19

Likewise, in Ca1 sample the background of Ca3 (8.5 cm deep profile) was subtracted to improve the identification of mineral phases. The results, consistent with the modelled hydrochemical data [2], pointed the presence of schwertmannite (5.8%) and jarosite (6.9%), with presence of

 doi:10.20944/preprints202409.2134.v

plumbojarosite (Pb0.5Fe3+3(SO4)2(OH)6) (Figure S2). Although distinguishing among these phases is challenging [41], these results were also checked with the chemical data (Table 2). In this case, a preferential retention of Pb can be observed, supporting DR-X interpretations. Regarding trace elements, SEP results (F3 and F4 SEP extractant) and potassium distribution among the fractions could indicate a relative affinity between both As-schwertmannite and Cu-jarosite. Additionally, other sulphate phases such as melanterite (FeSO4·7H2O; 4%), gypsum (74%), or phosphates like brushite (5.9%) are linked to Fe and Ca reactivity in this section. The hydrochemistry of the water column in Ca3 and deeper strata suggested that Fe di-sulfate species were leading [FeSO4+ (73%) and Fe (SO4)2− (14%)], supporting the formation of melanterite, which would increase the proportion of hydrolyzed species, promoting the precipitation of saturated Fe phases like schwertmannite and jarosite [54].

On the other hand, at this profile position, a low 2θ crest seems to indicate the presence of Al-phases like boehmite (3.4%, Table 3). According to the hydrochemical model, at pH values greater than 4 (10cm depth), and in line with the data described by [41], the presence of Al oxyhydroxides (alunite and basaluminite, among others) can be expected. As previously outlined, the substitution of Fe by Al becomes more noticeable in this section of the profile (Figure 4c). In fact, SEM data allowed the distinction of a common pattern of distribution of Al, S, and Mg (Figure 4d), which could imply the presence of other sulfate phases such as Epsomite (MgSO4) or pickeringite (MgAl2(SO4)4 2·2H2O). Although their presence cannot be confirmed, the SEP data also support this argument, as significant concentrations of Mg (280 mg/kg) associated with the labile fraction (F1) can be observed.

The samples at depths Ca4 and Ca5 did not show more Al-rich phases, except for the presence of diaspore, but in a low proportion (1.15% of the crystalline phases in sample Ca4). Both samples were characterized by the high presence of calcite from the reactive substrate, higher than 50% (Table 3, Figures S3, S4). Additionally, the Ca4 sample showed representative amounts of gypsum (44%) and dolomite (3%), probably derived from pH increase that could also promote the precipitation of this carbonate-type divalent metal phases in presence of high Mg concentration [2]. Calcite and gypsum are the most frequent phases in the final section of the DAS-Ca and in the DAS-Mg column (Table 3), due to the large amount of calcium-reactive available (evidenced by the high proportion in sample Ca5, Figure 4e). In fact, SEM study of the surface precipitates in the DAS-Mg column suggested that the white aggregates (Mg-SB) were essentially composed of gypsum (Figure 5a), while the green-blue ones (Mg-SV), also exhibited a nanocrystalline lattice composed of Fe, Cu and C (Figure 5b). XRD suggested this grid was composed by metal(II) hydroxide carbonate minerals (rosasite group, including malachite-Cu) and siderite.

Under the conditions of the DAS-Mg column with pH > 6, newly formed carbonate and bicarbonate phases could play an important role in removing divalent metals from solution [2]. The presence of dolomite in this section was explained by the dissolution of the reactive magnesia in the DAS-Mg. Thus, monohydrocalcite [CaCO3·(H2O)], malachite [Cu2CO3(OH)2], azurite [Cu3(CO3)2(OH)2], siderite and rhodochrosite [MnCO3] were identified (Table 3). The efficient removal of Cu and Mn within the initial centimeters of the DAS-Mg (Mg1, Figure 3b) was evident so subspherical Cu-C aggregates could be recognized by SEM (Figure 5c).

 doi:10.20944/preprints202409.2134.v

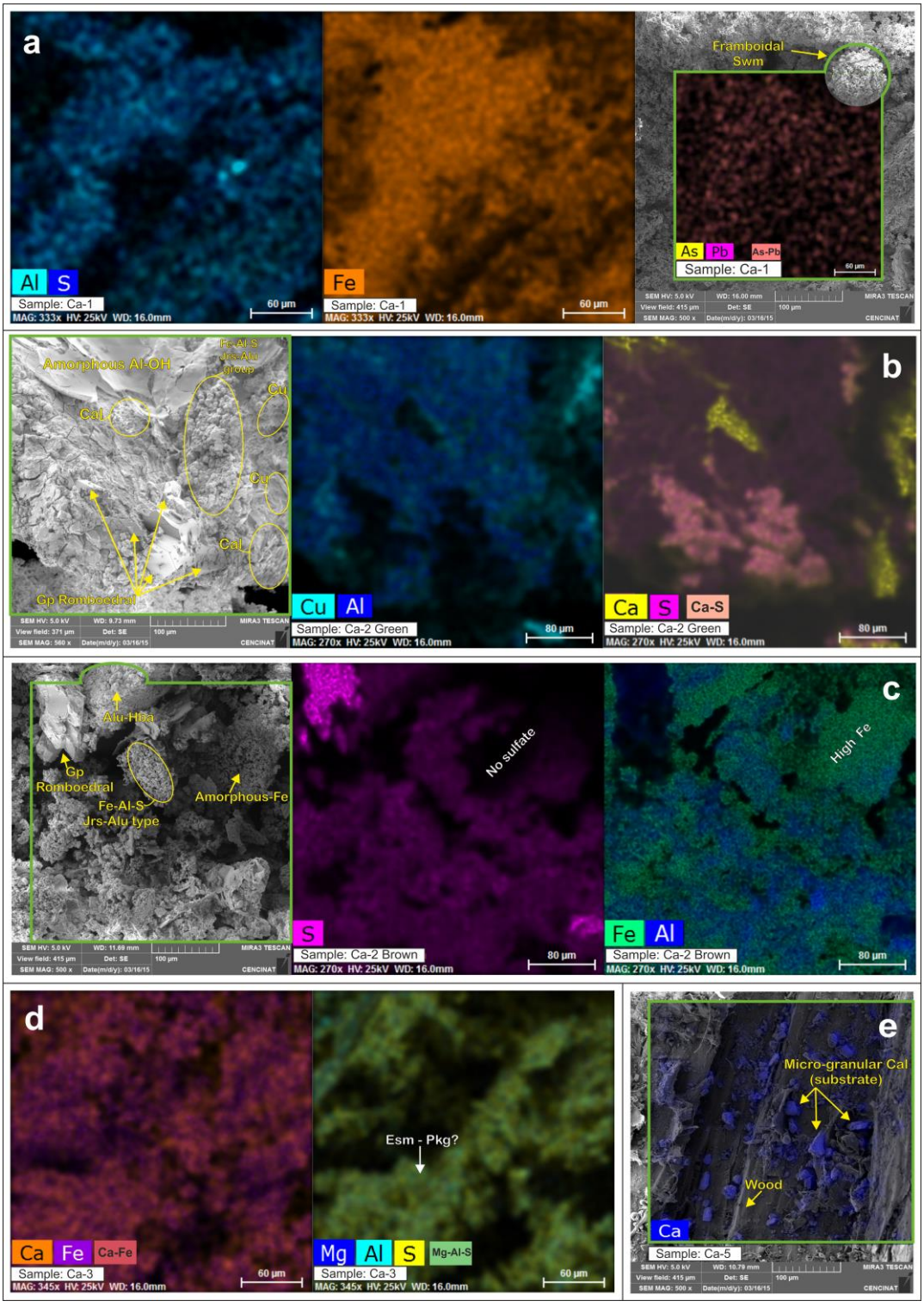

Figure 4. SEM Images revealing composition and morphology of mineralogical assemblages from DAS-Ca. The green frame highlights the correlation between the SE image and compositional mapping using Quantax. (a) Sample Ca1, where the relationship of Fe and Al with trace elements such as As and Pb can be observed. Framboidal aggregates of schwertmannite cam also observed. (b) Sample Ca2, showing Gp rhombohedral and the formation of aluminum hydroxides and copper carbonates in local alkaline conditions and (c) The presence of Fe (microcrystalline aggregates (<10 m) of Fe-Al-S, attributed to the Jarosite-Alunite group). The larger-sized spherical aggregates exhibit low concentrations of Fe (alunite-basaluminite). (d) Samples Ca-3 showing the presence of Mg-Al sulphates (identical compositional map) that could imply the formation of epsomite or pickeringite. (e) Microgranular calcite on the reactive substrate over wood shavings in sample Ca5.

 doi:10.20944/preprints202409.2134.v

Although iron chemistry is typically broad in more acidic environments (e.g., DAS-Ca), small amounts of available Fe associated with carbonate group as a divalent metal and precipitated as siderite [Fe2+(CO3)] (Figure 3b and S5; Table 3), representing 6.5% and 3.1% of the crystalline phases in samples Mg1 and Mg2, respectively. SEP results clearly revealed high concentrations of Cu, Fe, Mn, and Zn in the DAS-Mg (Figure 2g and 2h) associated with carbonate system (F2). Additionally, based on the hydrochemical data of these environments (high Mn concentrations) and the mineralogical interpretations of the Das-Mg samples, the presence of rhodochrosite can be confirmed (Figure 3b and 5S; 9% of the Mg2 sample).

According to [32], metal hydroxides rapidly precipitate in these experiments, while sulphates precipitate more slowly and progressively. Although the literature suggests the presence of brucite [Mg(OH)2], it only appeared in a negligible proportion (0.6% over the total crystalline phases of the sample Mg2, Figure S5) at the deepest part of the Mg-column. However, SEM data demonstrated the presence of Na and Mg associated, forming small-sized spherical aggregates (Figure 5d). This was also supported by the concentration of Mg and Na determined in F1 of DAS-Mg samples (Figure 2g-h), which evidenced carbonate-type divalent metal phases play an important role in the partition processes between AMD and solids in the final section of the treatment [2]. Moreover, the alkaline conditions facilitate the saturation of carbonated phases, such as calcite or dolomite, which could be recognized as subspherical aggregates of Ca-Mg, displaying the same compositional pattern as C (Figure 5d). These phases could play a role in coprecipitation-sorption processes, influencing the solubility of Zn, Mn, and other trace elements [56] (Jensen et al., 2002). In fact, the higher Zn and Mn concentrations were associated with the F2 of the Mg1 and Mg2 samples (516 and 465 g/kg of Zn and 13 and 75 g/kg of Mn, respectively). The data revealed that Zn is the divalent metal whose partition towards the solid phase undergoes in the late stages of the treatment (DAS-Mg) but it is depleted by carbonate mineral phases such as aurichalcite [(Zn, Cu2+)5 (CO3)2·(OH)6] (7% in the Mg2 samples). SEP data showed that 516 g/kg of Zn, and 906 g/Kg of Cu were trapped in the carbonated phases (F2) of Mg1 sample, supporting this assumption.

On the other hand, due to the high availability of sulphate hydroxides, newly formed phases linked to divalent metals such as brochantite [Cu4SO4(OH)6], antlerite [(Cu2+)3SO4(OH)4], goslarite [ZnSO4·7H2O], and anglesite [PbSO4], among others, are frequently described [47]. However, the mineralogical characterization of the samples is consistent with the hydrochemical model (Figure 3b in [2]) that shows low depletion of aqueous sulphated phases in the final section of the treatment. While hydrated sulphates are frequently described as the main controlling factor in the partitioning process of divalent metals such as Cu, Zn, or even Fe [57], no sulphate phases involving these elements were identified in the samples of the present study.

Finally, the bottom sample of the treatment ("Arenas del Pindo" – sandy drainage; Table 3 and Figure S6) is characterized by the presence of quartz (72%), albite (8.7%), K-feldspar (microcline-orthoclase 2.5%), and phyllosilicates (mainly biotite 12% and chlorite, 4% of the total). This mineralogy explains the presence of crystalline quartz in some samples such as Ca1 or Mg2, probably accidentally transferred along the samples during the columns opening process.

 doi:10.20944/preprints202409.2134.v

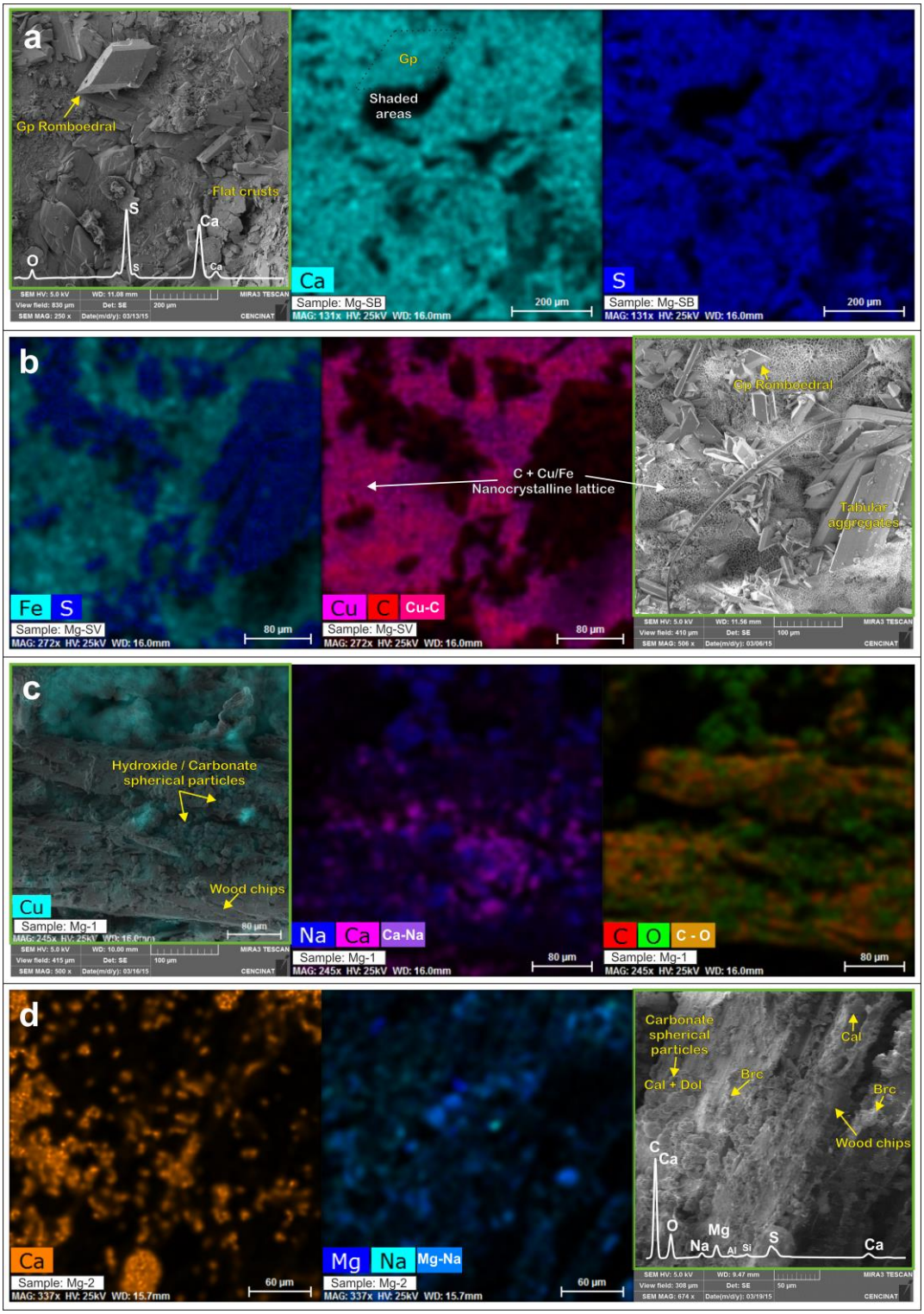

Figure 5. SEM Images revealing composition and morphology of mineralogical assemblages from DAS-Mg. The green frame highlights the correlation between the SE image and compositional mapping using Quantax. (a-b) both precipitates collected on the surface of the residue from the DAS-Mg column, white (SB) and green (SV), respectively, showing diverse gypsum crystallization form. Also, (b) presents a nanocrystalline lattice of Cu-Fe carbonate. (c) Sample Mg-1, where the relation of divalent metals and carbonate can be observed. (d) Samples Mg2 showing the presence subspherical aggregates of Ca-Mg (calcite and dolomite) and another spherical particulate with high Na-Mg

 doi:10.20944/preprints202409.2134.v

4.3. Possible Environmental Implication of Residues Management

In the literature, inconsistent predictions regarding the stability of PTE (Potentially Toxic Elements) content in AMDp have been reported, depending on various factors such as the type of leaching test employed, the extracting agent used, the duration of the test, the presence of oxygen, and the regulatory criteria applied [58]. In order to make more accurate predictions about how these residues will behave in the environment and to carry out an appropriate sustainable management option, metal stability in multi-step passive treatment systems require a comprehensive study [17], combining chemical and mineralogical characterization [59,60]. Additionally, this approach could indicate the potential economic benefits of the generated residues [61].

SEP is commonly employed to assess the possible movement of pollutants in different simulated environmental scenarios. However, it is crucial to carefully select and test reagents to prevent incomplete extraction and potential alterations in the outcomes of the experiment [62; 58]. In this sense, studies have been carried out on samples containing high levels of iron oxides and iron oxyhydroxysulfates [21], and latter improved by [35] for phases like hydrobasaluminite when Al content is associated to Fe(III) minerals. This procedure delineates five distinct fractions: water-soluble, exchangeable, poorly crystallized oxyhydroxides, well-crystallized oxyhydroxides, and residual. The distinction among these fractions depends on their crystallinity, which plays a key role in determining the release of contaminants.

Based on this improved SEP, this study has evaluated the potential leaching of PTEs from AMDp in the different weathering scenarios (Figure 6) by comparing with limit values established by the criterion continuous concentration (CCC) from the recommended water quality criteria adopted by the European Community [63]. This value represents a potential negative effect for the aquatic life when uncontrolled leachates are generated from an inappropriate disposal of the AMDp. The proposed scenarios are Scenario 1: Contact of the residue with rainwater (emulated by F1 SEP fraction) which may occur in uncovered disposal facilities and are considered highly dangerous to the environment according to regulations [64]; Scenario 2: Interaction between the residue and weak acidic leachates under reducing conditions (F1+F2 fraction). These conditions are relevant to scenarios such as underground disposal facilities; and finally, Scenario 3: Exposure of the residues to weak acidic leachates in oxidizing environments (F1+F3+F4 fraction). These conditions aim to simulate disposal scenarios in surface impoundments or waste piles, as previously has been described by [12].

The data suggests that, although some samples may occasionally fall below the CCC limit, when the resulting whole-body residue from any DAS system is disposed of, it could pose danger to aquatic ecosystems and the life associated with them. In scenario 1 (exposure to rainfall), Pb, Zn, Al, and Fe exceed the proposed values for DAS-Ca, while Cd, Cr, Zn, and Fe behave similarly for DAS-Mg. For the rest of the more aggressive conditions, scenario 2 (underground disposal) and scenario 3 (surface impoundments or waste piles), the AMD residues generate leachates that surpass the threshold for most of the elements studied, making them incompatible with aquatic life. In this regard, these metal-rich residues from passive treatments (both laboratory scale and field scale), when stored in an oxidizing environment, demonstrated significant leaching of metals and sulfates [58; 65]. Several studies have shown that residues from Fe-rich AMD are unstable and have a high risk of leaching. They should be stored underwater or in a neutral pH environment to prevent contamination release and ensure safe disposal [5; 6]. Meanwhile, specific studies on MgO-DAS also recommend storing them in a dry (not mix acidic or alkaline waters) environment [15]. More recent studies suggest that in addition to being stored under anoxic conditions in the presence of water to prevent the formation of new AMD, these residues should undergo stabilization/solidification before any storage [8].

 doi:10.20944/preprints202409.2134.v

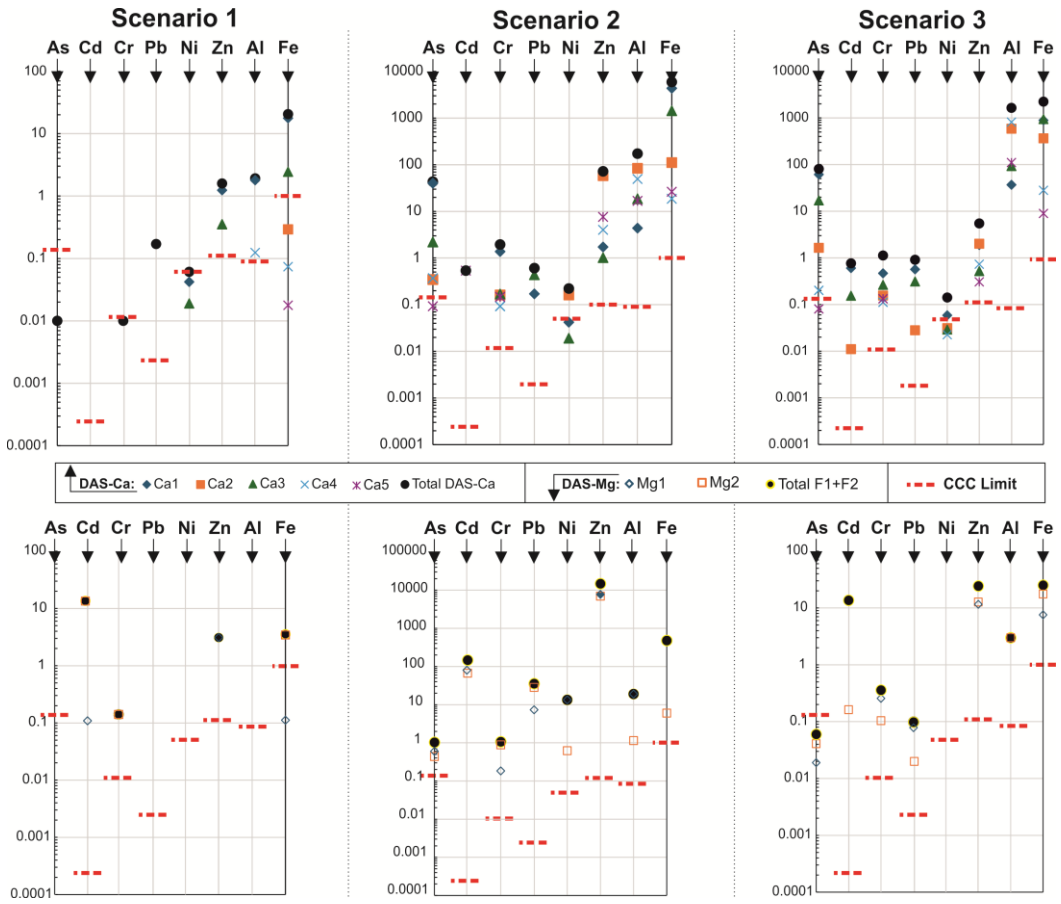

Figure 6. Charts showing the leached concentrations of As, Cd, Cr, Pb, Ni, Zn, Al and Fe in the different weathering scenarios from DAS-Ca (upper) and DAS-Mg (down) residues. The Continuous Concentration Criterion (CCC limit) from US EPA National Recommended Water Quality Criteria is also shown with comparison purposes. Data in mg/L.

In addition, Table 4 presents the regulatory limits for waste acceptance at landfills in the EU [64] in comparison to the concentrations of elements detected in AMDp (DAS-Ca and DAS-Mg) following the F1 leaching fraction. This fraction denotes the metals and metalloids capable of mobilization upon contact with water and are considered as the leaching limit values to be applied to the waste for storage in the three types of landfills proposed by the Royal Decree 646/2020, under the auspices of the [64].

Table 4. Comparison between AMDp and the regulatory criteria for the acceptance of waste at landfills type and their classification of hazardousness (Council Decision, 2003/33/EC).

Landfill type		As	Ba	Cd	Cr	Cu	Ni	Pb	Zn	Sulfate
	DAS-Ca	< d.l	< d.l	< d.l	0.7	50	4.0	10	104	<5000
	DAS-Mg	< d.l	< d.l	901	9.4	164	< d.l	< d.l	206	<5000
Inert wastes		0.5	20	0.04	0.5	2.0	0.4	0.5	4.0	1000
Non-Hazardous wastes		**2.0**	**100**	**1**	**10**	**50**	**10**	**10**	**50**	**20000**
Hazardous wastes		25	300	5	70	100	50	50	200	50000

< d.l. Below detection limit. Data in mg/kg.

According to the results obtained, the DAS-Ca residues would be classified as hazardous since the concentration of Zn (104 mg/kg) exceeds the reference value, while Cu (50 mg/kg) and Pb (10 mg/kg) are at the limit value. Meanwhile, the precipitates of the DAS-Mg would pose storage issues in landfills due to the excessive leached concentrations of Cd (901), Cu (164), and Zn (206 mg/kg). Under these circumstances, the EU regulation [64] recommends additional treatment (such as further neutralization, encapsulation, etc.) before the storage of these materials in any type of regulated landfill. Also, recent directives established and emphasized, in general terms, the necessity of subjecting waste destined for landfills to appropriate pretreatment [66], considering as an essential

 doi:10.20944/preprints202409.2134.v

requirement to ensure that landfill operations are conducted without endangering human health and the environment. Additionally, in accordance with the circularity principle, it is important to note that these treatments generate metal-rich solid residues considered generally hazardous wastes, but that can also present an opportunity for the potential recovery of metals and other critical elements [58; 67-68]. In this regard, the European Regional Development Fund (FEDER, 2021-2027) aims to enhance these efforts by fostering the transition to a circular and resource-efficient economy (Raw Materials Initiative) through the generation of added value from waste. This initiative contributes to reducing the amount of waste sent to landfills and conserving natural resources by promoting reuse and recycling.

5. Conclusions

The mineralogy of solid residues from the DAS system experience with Ecuadorian AMD was consistent with the basic principles of metal retention from acidic solutions and helped the interpretation of geochemical results and modellings. Elements like Fe and Al were retained in the DAS-Ca column, while most divalent metals fractionated towards the solid phase in the DAS-Mg.

Among the minerals that retained trivalent elements, oxyhydroxysulfates such as schwertmannite and the jarosite-alunite group were primarily responsible for their fractionation towards the solid phase. In this process of mineral formation, other trace elements with diverse charges were retained through adsorption-coprecipitation mechanisms (As, Cr, Cu, Pb, and Zn). Additionally, sulfated efflorescent salts such as coquimbite and gypsum were responsible for removing sulfate from solution.

Fractionation of divalent metals (Cu, Zn, and Mn) predominantly occurred in the DAS-Mg column, and it was controlled by the formation of carbonated phases (identified through XRD and SEM studies). In the initial stages of DAS-Mg, phases rich in Cu-Zn from the azurite-malachite group were abundantly formed, while other discrete phases such as rhodochrosite (Mn) appeared accompanying neoformed calcite, monohydrocalcite, and dolomite when Mg supply increased in the column. Hydroxides of divalent metals have frequently been described as the main mechanism for controlling metal load in passive treatment systems DAS type; however, although they are not absent, the results of this study suggest that newly formed carbonate and bicarbonate phases are the most evident neutralization mechanism trapping the metallic charge. This result confirms the initial hypothesis of the metal fractionation processes according to the hydrochemical model proposed by [2], highlighting the key role of carbonates in removing divalent metals from the AMD solution.

The leachates from SEP were analyzed against the limits set by the continuous concentration criterion (CCC) to assess potential aquatic life exposure to contaminants in various disposal scenarios. In these scenarios (disposal in superficial environmental conditions, in underground facilities, and in surface impoundments or waste piles) the established values were exceeded for PTE including As, Cd, Cr, Pb, Ni, Zn (excluding punctual samples of the profile). According to the regulatory normative, none of the DAS residues could be defined as inert wastes. DAS-Ca solids could be classified as non-hazardous wastes for most elements (only Zn poses risk). Residues from DAS-Mg exceed the hazard threshold for Cd, Cu, and Zn, indicating a significant environmental risk for all landfill options, emphasizing the need to prevent waste from directly contacting leaching solutions.

Combining different analytical and management approaches could improve waste management practices and mitigate potential environmental risks by providing a more comprehensive understanding of the composition, behavior and potential environmental impacts of these residues. Efforts should focus on accurately characterizing waste to promote viable solutions aimed at reducing the volume of wastes sent to landfill by using them as a new source of metals and other critical elements.

Supplementary Materials: The following supporting information can be downloaded at: www.mdpi.com/xxx/s1, Figures S1 to S6: DRX pattern of samples in the DAS-Ca: S1 (Ca2, 7.5 cm); S2 (Ca3, 8.5 cm); S3 (Ca4, 10 cm); S4 (Ca5, 15 cm) and DAS-Mg: S5 (Mg2, 12 cm), as well as S6 (Pindo, drain-sand of the bottom columns), showing the main mineral phases identified* and their correlation with the patterns obtained

from database by Match. Mineral symbol according to IMA–CNMNC. * Semiquantitative results have been improved by Rietveld refinement (See also Table 3).

Author Contributions: Conceptualization, J.D.; methodology, O. L. and D.A.; validation, J.D.; C.B-B.; D.A.; investigation, J.D., C.B-B, D.A; resources, D.A.; writing—original draft preparation, O.L.; writing—review and editing, J.D. and C.B-B; visualization, J.D. and C.B-B; supervision, J.D. and C.B-B; project administration, J.D. and D.A.; funding acquisition, J.D. All authors have read and agreed to the published version of the manuscript.

Funding: This work was supported by PROMETEO Ecuadorian program (Secretary of Superior Education, Science, Technology and Innovation) in the framework of the project "Experiencia Piloto en la Remediación y Mitigación de la Oxidación de Sulfuros y la Generación de AMD en Relaveras del Distrito Minero de Zaruma-Portovelo" by mean of the postdoctoral contract nº 20140411 BP.

Data Availability Statement: Dataset available on request from the authors.

Acknowledgments: The authors acknowledge the material and human resources displayed from INIGEMM (Ecuadorian National Research Institute of Geology, Mining and Metallurgy) and US (Seville University). Diana Ayala Diana Ayala thanks Dr. Cumbal for the support in studying the samples using SEM at the Center for Nanoscience and Nanotechnology (CENCINAT).

Conflicts of Interest: The authors declare that they have no known competing financial interests or personal relationships that could have appeared to influence the work reported in this paper.

References

1. Nordstrom, D.K., Blowes, D.W., Ptacek, C.J. Hydrogeochemistry and microbiology of mine drainage: An update. *Appl. Geochem.* **2015**, 57, 3–16. https://doi.org/https://doi.org/10.1016/j.apgeochem.2015.02.008
2. Delgado, J., Barba-Brioso, C., Ayala, D., Boski, T., Torres, S., Calderón, E., López, F. Remediation experiment of Ecuadorian acid mine drainage: geochemical models of dissolved species and secondary minerals saturation. *ESPR* **2019**. https://doi.org/10.1007/s11356-019-06539-3.
3. Park, I., Tabelin, C.B., Magaribuchi, K., Seno, K., Ito, M., Hiroyoshi, N. Suppression of the release of arsenic from arsenopyrite by carrier-microencapsulation using Ti-catechol complex. *J Hazard Mater* **2018**, 344, 322–332.

https://doi.org/https://doi.org/10.1016/j.jhazmat.2017.10.025.

4. Jouini, M., Rakotonimaro, T. V, Neculita, C.M., Genty, T., Benzaazoua, M. Stability of metal-rich residues from laboratory multi-step treatment system for ferriferous acid mine drainage. *ESPR* **2019**, 26, 588–601. https://doi.org/10.1007/s11356-019-04608-1.
5. Genty, T., Bussière, B., Benzaazoua, M., Zagury, G.J. Capacity of Wood Ash Filters to Remove Iron from Acid Mine Drainage: Assessment of Retention Mechanism. *Mine Water Environ* **2012**, 31, 273–286. https://doi.org/10.1007/s10230-012-0199-z.
6. Neculita, C.-M., Zagury, G.J., Bussière, B. Effectiveness of sulfate-reducing passive bioreactors for treating highly contaminated acid mine drainage: II. Metal removal mechanisms and potential mobility. *Appl. Geochem* **2008**, 23, 3545–3560.

https://doi.org/https://doi.org/10.1016/j.apgeochem.2008.08.014.

7. Rakotonimaro, T. V, Neculita, C.M., Bussière, B., Genty, T., Zagury, G.J. Performance assessment of laboratory and field-scale multi-step passive treatment of iron-rich acid mine drainage for design improvement. *ESPR* **2018**, 25, 17575–17589. https://doi.org/10.1007/s11356-018-1820-x.
8. Jouini, M., Benzaazoua, M., Neculita, C.M., Genty, T. Performances of stabilization/solidification process of acid mine drainage passive treatment residues: Assessment of the environmental and mechanical behaviors. *J Environ Manage* **2020**, 269, 110764.

https://doi.org/https://doi.org/10.1016/j.jenvman.2020.110764.

9. Skousen, J., Zipper, C.E., Rose, A., Ziemkiewicz, P.F., Nairn, R., McDonald, L.M., Kleinmann, R.L. Review of Passive Systems for Acid Mine Drainage Treatment. *Mine Water Environ* **2017**, 36, 133–153. https://doi.org/10.1007/s10230-016-0417-1.
10. Ayora, C., Caraballo, M.A., Macias, F., Rötting, T.S., Carrera, J., Nieto, J.-M. Acid mine drainage in the Iberian Pyrite Belt: 2. Lessons learned from recent passive remediation experiences. *ESPR* **2013**, 20, 7837–7853. https://doi.org/10.1007/s11356-013-1479-2.
11. Caraballo, M.A., Macías, F., Nieto, J.M., Castillo, J., Quispe, D., Ayora, C. Hydrochemical performance and mineralogical evolution of a dispersed alkaline substrate (DAS) remediating the highly polluted acid mine drainage in the full-scale passive treatment of Mina Esperanza (SW Spain). *Am Min* **2011**, 96, 1270–1277. https://doi.org/doi:10.2138/am.2011.3752.
12. Macías, F., Pérez-López, R., Caraballo, M.A., Cánovas, C.R., Nieto, J.M. Management strategies and valorization for waste sludge from active treatment of extremely metal-polluted acid mine drainage: A

contribution for sustainable mining. *J Clean Prod* **2017**, 141, 1057–1066. https://doi.org/https://doi.org/10.1016/j.jclepro.2016.09.181.

13. Rakotonimaro, T. V, Neculita, C.M., Bussière, B., Zagury, G.J. Effectiveness of various dispersed alkaline substrates for the pre-treatment of ferriferous acid mine drainage. *Appl. Geochem*. **2016**, 73, 13–23. https://doi.org/https://doi.org/10.1016/j.apgeochem.2016.07.014.
14. Rötting, T.S., Thomas, R.C., Ayora, C., Carrera, J. Passive Treatment of Acid Mine Drainage with High Metal Concentrations Using Dispersed Alkaline Substrate. *J Environ Qual* **2008**, 37, 1741–1751. https://doi.org/https://doi.org/10.2134/jeq2007.0517.
15. Macías, F., Caraballo, M.A., Nieto, J.M., Rötting, T.S., Ayora, C. Natural pretreatment and passive remediation of highly polluted acid mine drainage. *J Environ Manage* **2012**, 104, 93–100. https://doi.org/https://doi.org/10.1016/j.jenvman.2012.03.027.
16. Rakotonimaro, T. V, Neculita, C.M., Bussière, B., Benzaazoua, M., Zagury, G.J. Recovery and reuse of sludge from active and passive treatment of mine drainage-impacted waters: a review. *ESPR* **2017**, 24, 73-91. https://doi.org/10.1007/s11356-016-7733-7.
17. Jouini, M., Benzaazoua, M., Neculita, C.M., Genty, T. Performances of stabilization/solidification process of acid mine drainage passive treatment residues: Assessment of the environmental and mechanical behaviors. *J Environ Manage* **2020**, 269, 110764.
https://doi.org/https://doi.org/10.1016/j.jenvman.2020.110764.
18. Fanfani, L., Zuddas, P., Chessa, A. Heavy metals speciation analysis as a tool for studying mine tailings weathering. *J Geochem Explor* **1997**, 58, 241–248. https://doi.org/https://doi.org/10.1016/S0375-6742(96)00059-3.
19. Khorasanipour, M., Tangestani, M.H., Naseh, R., Hajmohammadi, H. Hydrochemistry, mineralogy and chemical fractionation of mine and processing wastes associated with porphyry copper mines: A case study from the Sarcheshmeh mine, SE Iran. *Appl. Geochem.* **2011**, 26, 714–730. https://doi.org/https://doi.org/10.1016/j.apgeochem.2011.01.030.
20. Ribeta, I., Ptacek, C.J., Blowes, D.W., Jambor, J.L. The potential for metal release by reductive dissolution of weathered mine tailings. *J Contam Hydrol* **1995**, 17, 239–273. https://doi.org/https://doi.org/10.1016/0169-7722(94)00010-F.
21. Dold, B. Speciation of the most soluble phases in a sequential extraction procedure adapted for geochemical studies of copper sulfide mine waste. *J Geochem Explor* **2003**, 80, 55–68. https://doi.org/https://doi.org/10.1016/S0375-6742(03)00182-1.
22. Sahuquillo, A., Rigol, A., Rauret, G. Overview of the use of leaching/extraction tests for risk assessment of trace metals in contaminated soils and sediments. *TrAC* **2003**, 22, 152–159. https://doi.org/https://doi.org/10.1016/S0165-9936(03)00303-0.
23. U.S. EPA (U.S. Environmental Protection Agency). 2019. Guidelines for Human Exposure Assessment. (EPA/100/B-19/001). Washington, D.C.: Risk Assessment Forum, U.S. EPA.
24. Betancourt, O., Narváez, A., Roulet, M. Small-scale Gold Mining in the Puyango River Basin,Southern Ecuador: A Study of Environmental Impacts andHuman Exposures. *Ecohealth* **2005**, 2, 323–332. https://doi.org/10.1007/s10393-005-8462-4.
25. Delgado, Joaquín, Ayala, Di., Páez, H.S. Treatment system to improve the drainage water quality of the Puyango River environmental liabilities. *Geogaceta* **2018**, 64, 63–66.
26. Delgado, J, Barba-Brioso, C., Boski, T. Mine wastes characterisation and experimental design of a controlled tailing storage in the Zaruma-Portovelo mining district (SE Ecuador). *Geogaceta* **2018**, 64, 135–138.
27. Guimaraes, J.R.D., Betancourt, O., Miranda, M.R., Barriga, R., Cueva, E., Betancourt, S. Long-range effect of cyanide on mercury methylation in a gold mining area in southern Ecuador. *STOTEN* **2011**, 409, 5026–5033. https://doi.org/https://doi.org/10.1016/j.scitotenv.2011.08.021.
28. Tarras-Wahlberg, N.H., Flachier, A., Lane, S.N., Sangfors, O. Environmental impacts and metal exposure of aquatic ecosystems in rivers contaminated by small scale gold mining: the Puyango River basin, southern Ecuador. *STOTEN* **2001**, 278, 239–261. https://doi.org/https://doi.org/10.1016/S0048-9697(01)00655-6.
29. Tarras-Wahlberg, N.H., Lane, S.N. Suspended sediment yield and metal contamination in a river catchment affected by El Niño events and gold mining activities: the Puyango river basin, southern Ecuador. *Hydrol Process* **2003**, 17, 3101–3123. https://doi.org/https://doi.org/10.1002/hyp.1297.
30. Rötting, T.S., Ayora, C., Carrera, J. Improved Passive Treatment of High Zn and Mn Concentrations Using Caustic Magnesia (MgO): Particle Size Effects. *Environ Sci Technol* **2008**, 42, 9370–9377. https://doi.org/10.1021/es801761a.
31. Cabrera, G., Pérez, R., Gómez, J.M., Ábalos, A., Cantero, D. Toxic effects of dissolved heavy metals on Desulfovibrio vulgaris and Desulfovibrio sp. strains. *J Hazard Mater* **2006**, 135, 40–46. https://doi.org/https://doi.org/10.1016/j.jhazmat.2005.11.058.
32. Cortina, J.L., Lagreca, I.H., de Pablo, J., Cama, J., Ayora, C. Passive in situ remediation of metal-polluted water with caustic magnesia: evidence from column experiments. *Environ Sci Technol* **2003**, 37 9, 1971–7.

33. Gibert, O., de Pablo, J., Cortina, J.L., Ayora, C. Sorption studies of Zn(II) and Cu(II) onto vegetal compost used on reactive mixtures for in situ treatment of acid mine drainage. *Water Res* **2005**, 39, 2827–2838. https://doi.org/https://doi.org/10.1016/j.watres.2005.04.056.
34. Rötting, T.S., Cama, J., Ayora, C., Cortina, J.L., Pablo, J. De. Use of caustic magnesia to remove cadmium, nickel, and cobalt from water in passive treatment systems: Column experiments. *Environ Sci Technol* **2006**, 40, 6438–6443. https://doi.org/10.1021/ES061092G.
35. Caraballo, M.A., Rötting, T.S., Nieto, J.M., Ayora, C. Sequential extraction and DXRD applicability to poorly crystalline Fe- and Al-phase characterization from an acid mine water passive remediation system. *Am Min* **2009**, 94, 1029–1038. https://doi.org/doi:10.2138/am.2009.3137.
36. Delgado, J., Barba-Brioso, C., Nieto, J.M., Boski, T. Speciation and ecological risk of toxic elements in estuarine sediments affected by multiple anthropogenic contributions (Guadiana saltmarshes, SW Iberian Peninsula): I. Surficial sediments. *STOTEN* **2011**, 409. https://doi.org/10.1016/j.scitotenv.2011.06.013.
37. Tessier, A., Campbell, P.G.C., Bisson, M. Sequential extraction procedure for the speciation of particulate trace metals. *Anal Chem* **1979**, 51, 844–851. https://doi.org/10.1021/ac50043a017.
38. Dold, B. Speciation of the most soluble phases in a sequential extraction procedure adapted for geochemical studies of copper sulfide mine waste. *J Geochem Explor* **2003**, 80, 55–68. https://doi.org/https://doi.org/10.1016/S0375-6742(03)00182-1.
39. Sahuquillo, A., Rigol, A., Rauret, G. Overview of the use of leaching/extraction tests for risk assessment of trace metals in contaminated soils and sediments. *TrAC* **2003**, 22, 152–159. https://doi.org/https://doi.org/10.1016/S0165-9936(03)00303-0.
40. Hernández, J., Meurer, E. Óxidos de hierro en los suelos: sus propiedades y su caracterización con énfasis en los estudios de retención de fósforo. *Agrociencia* **1997**, 1, 1-14.
41. Sánchez-España, J., Yusta, I., Gray, J., Burgos, W.D. Geochemistry of dissolved aluminum at low pH: Extent and significance of Al–Fe(III) coprecipitation below pH 4.0. *Geochim Cosmochim Acta* **2016**, 175, 128–149. https://doi.org/10.1016/J.GCA.2015.10.035.
42. Hammarstrom, J.M., Seal, R.R., Meier, A.L., Kornfeld, J.M. Secondary sulfate minerals associated with acid drainage in the eastern US: recycling of metals and acidity in surficial environments. *Chem Geol* **2005**, 215, 407–431. https://doi.org/10.1016/J.CHEMGEO.2004.06.053.
43. Marescotti, P., Carbone, C., Comodi, P., Frondini, F., Lucchetti, G. Mineralogical and chemical evolution of ochreous precipitates from the Libiola Fe–Cu-sulfide mine (Eastern Liguria, Italy). *Appl Geochem* **2012**, 27, 577–589. https://doi.org/https://doi.org/10.1016/j.apgeochem.2011.12.024.
44. Nordstrom, D.K., Alpers, C.N. 1999. Geochemistry of Acid Mine Drainage. The Environmental Geochemistry of Mineral Deposits.
45. Delgado, J., Sarmiento, A.M., Condesso De Melo, M.T., Nieto, J.M. Environmental impact of mining activities in the southern sector of the Guadiana Basin (SW of the Iberian Peninsula). *Water Air Soil Pollut* **2009**, 199. https://doi.org/10.1007/s11270-008-9882-x.
46. Baes, C.F., Mesmer, R.S. 1977. The Hydrolysis of Cations. John Wiley & Sons, New York, London, Sydney, Toronto 1976. 489 pp., Berichte der Bunsengesellschaft für physikalische Chemie. John Wiley & Sons, Ltd. https://doi.org/https://doi.org/10.1002/bbpc.19770810252.
47. Carbone, C., Dinelli, E., Marescotti, P., Gasparotto, G., Lucchetti, G. The role of AMD secondary minerals in controlling environmental pollution: Indications from bulk leaching tests. *J Geochem Explor* **2013**, 132, 188–200. https://doi.org/10.1016/J.GEXPLO.2013.07.001.
48. Zachara, J.M., Cowan, C.E., Resch, C.T. Sorption of divalent metals on calcite. *Geochim Cosmochim Acta* **1991**, 55, 1549–1562. https://doi.org/https://doi.org/10.1016/0016-7037(91)90127-Q.
49. Papassiopi, N., Zaharia, C., Xenidis, A., Adam, K., Liakopoulos, A., Romaidis, I. Assessment of contaminants transport in a watershed affected by acid mine drainage, by coupling hydrological and geochemical modeling tools. *Miner Eng* **2014**, 64, 78–91. https://doi.org/https://doi.org/10.1016/j.mineng.2014.04.002.
50. Hudson-Edwards, K.A., Jamieson, H.E., Lottermoser, B.G. Mine wastes: past, present, future. *Elements* **2011**, 7, 375–380.
51. Behum, P. and Kim, K., 1999, "Workshop for the application of passive technology to the treatment of acid mine drainage," Office of Surface Mines, Alton, Illinois, presented at Jasper, Indiana.
52. Barba-Brioso, C., Martín, D., Romero-Baena, A., Campos, P., Delgado, J. Revalorisation of Fine Recycled Concrete in Acid Mine Water Treatment: A Challenge to a Circular Economy. *Minerals* **2023**, 13. https://doi.org/10.3390/min13081028.
53. Katsioti, M., Tsakiridis, P.E., Leonardou-Agatzini, S., Oustadakis, P. Examination of the jarosite–alunite precipitate addition in the raw meal for the production of sulfoaluminate cement clinker. *J Hazard Mater* **2006**, 131, 187–194. https://doi.org/https://doi.org/10.1016/j.jhazmat.2005.09.028.
54. Shum, M., Lavkulich, L. Speciation and solubility relationships of Al, Cu and Fe in solutions associated with sulfuric acid leached mine waste rock. *Environ Geol* **1999**, 38, 59–68. https://doi.org/10.1007/s002540050401.

55. Warr, L.N. IMA–CNMNC approved mineral symbols. *Mineral Mag* **2021**, 85, 291–320. DOI: https://doi.org/10.1180/mgm.2021.43.
56. Jensen, D.L., Boddum, J.K., Tjell, J.C., Christensen, T.H. The solubility of rhodochrosite ($MnCO_3$) and siderite ($FeCO_3$) in anaerobic aquatic environments. Appl Geochem **2002**, 17, 503–511. https://doi.org/https://doi.org/10.1016/S0883-2927(01)00118-4.
57. Jambor, J.L., Nordstrom, D.K., Alpers, C.N. Metal-sulfate Salts from Sulfide Mineral Oxidation. *Rev Mineral Geochem* **2000**, 40, 303–350. https://doi.org/10.2138/rmg.2000.40.6.
58. Mehdaoui, H.Y., Guesmi, Y., Jouini, M., Neculita, C.M., Pabst, T., Benzaazoua, M. Passive treatment residues of mine drainage: Mineralogical and environmental assessment, and management avenues. *Miner Eng* **2023**, 204, 108362. https://doi.org/https://doi.org/10.1016/j.mineng.2023.108362.
59. Lounate, K., Coudert, L., Genty, T., Mercier, G., Blais, J.F. Geochemical behavior and stabilization of spent sulfate-reducing biofilter mixtures for treatment of acid mine drainage. *STOTEN* **2020**, 718, 137394. https://doi.org/https://doi.org/10.1016/j.scitotenv.2020.137394..
60. McCann, J.I., Nairn, R.W. Characterization of residual solids from mine water passive treatment oxidation ponds at the tar creek superfund site, Oklahoma, USA: Potential for reuse or disposal. *Clean. Waste Syst.* **2022**, 3, 100031. https://doi.org/https://doi.org/10.1016/j.clwas.2022.100031.
61. Jouini, M., Benzaazoua, M., Neculita, C.M., 2022. Chapter 12 - Stabilization/solidification of acid mine drainage treatment sludge, in: Tsang, D.C.W., Wang, L. (Eds.), Low Carbon Stabilization and Solidification of Hazardous Wastes. Elsevier, pp. 175–199. https://doi.org/https://doi.org/10.1016/B978-0-12-824004-5.00003-7.
62. Caraballo, M.A., Serna, A., Macías, F., Pérez-López, R., Ruiz-Cánovas, C., Richter, P., Becerra-Herrera, M. Uncertainty in the measurement of toxic metals mobility in mining/mineral wastes by standardized BCR®SEP. *J Hazard Mater* **2018**, 360, 587–593.
https://doi.org/https://doi.org/10.1016/j.jhazmat.2018.08.046.
63. U.S. EPA (U.S. Environmental Protection Agency). (2016). National Recommended Water Quality Criteria - Aquatic Life Criteria Table. https://www.epa.gov/wqc/national-recommended-water-quality-criteria-aquatic-life-criteria-table
64. EC Decision 2003/33/CE, 16/01/2003. Council decision of 19 december 2002 establishing criteria and procedures for the acceptance of waste at landfills pursuant to Article16 of an Annex II to Directive 1999/31/EC. Off. J. L 011, 0027-0049.
65. Vasquez, Y., Neculita, C.M., Caicedo, G., Cubillos, J., Franco, J., Vásquez, M., Hernández, A., Roldan, F. Passive multi-unit field-pilot for acid mine drainage remediation: Performance and environmental assessment of post-treatment solid waste. *Chemosphere* **2022**, 291, 133051. https://doi.org/https://doi.org/10.1016/j.chemosphere.2021.133051.
66. Real Decreto 646/2020, de 7 de julio, por el que se regula la eliminación de residuos mediante depósito en vertedero. Boletín Oficial del Estado, n. 187, de 8 de julio de 2020.
67. Vass, C.R., Noble, A., Ziemkiewicz, P.F. The Occurrence and Concentration of Rare Earth Elements in Acid Mine Drainage and Treatment By-products: Part 1—Initial Survey of the Northern Appalachian Coal Basin. *Min Metall Explor* **2019**, 36, 903–916. https://doi.org/10.1007/s42461-019-0097-z.
68. Vaziri Hassas, B., Shekarian, Y., Rezaee, M., Pisupati, S. V. Selective recovery of high-grade rare earth, Al, and Co-Mn from acid mine drainage treatment sludge material. *Miner Eng* **2022**, 187, 107813.
https://doi.org/https://doi.org/10.1016/j.mineng.2022.107813.